J Mater Sci: Mater Electron (2013) 24:3905–3913
DOI 10.1007/s10854-013-1337-5

Phase transformation and grain orientation of Cu–Sn intermetallic compounds during low temperature bonding process

Chunjin Hang · Yanhong Tian · Rui Zhang · Dongsheng Yang

Received: 11 April 2013 / Accepted: 4 June 2013 / Published online: 27 June 2013
© Springer Science+Business Media New York 2013

Abstract The interconnection lengths between the stacked chips in three-dimensional (3D) package are a few of microns, hence the solder joints for the stacked chips joining are mainly composed by intermetallic compounds (IMCs) after reflow processes. To evaluate the phase transformation of Cu–Sn IMCs in the small interconnection joints, the Cu/Sn/Cu structures were bonded with different bonding times at various temperatures in argon gas atmosphere in this study. Scanning electron microscope and energy-dispersive X-ray were used to observe the joint interfacial microstructures and electron back scattering diffraction was used to identify the grain orientations in the joints. Scalloped Cu_6Sn_5 grains were found to be initially formed on the Cu substrates at the early stage. A lot of small Cu_6Sn_5 grains formed on the surfaces of the big scallop Cu_6Sn_5 grains. Those small grains gradually grew up to merge into the big Cu_6Sn_5 grains. With longer reflow time, the Cu_6Sn_5 grains initiated at both side of Cu substrate continued to grow up and started to contact with each other. Meantime, the different Cu_6Sn_5 grains with different grain orientations have merged into some bigger grains. The Cu_3Sn grains formed between Cu_6Sn_5 layers and Cu substrates have further developed at the expense of the depletion of Cu_6Sn_5. Most of columnar Cu_3Sn grains were vertical to Cu substrate surface and their grain sizes were 1–5 μm. With 960 min at 300 °C, the pure Cu_3Sn IMC joint has formed. The Cu_3Sn grains in IMC joint had different grain orientations and a contact line was observed in the middle of the Cu_3Sn IMC joint.

C. Hang · Y. Tian (✉) · R. Zhang · D. Yang
State Key Lab of Advanced Welding and Joining, Harbin Institute of Technology, Harbin 150001, China
e-mail: tianyh@hit.edu.cn

1 Introduction

Three-dimensional (3D) package is considered as the predominant interconnection technology in the coming era of semiconductor industry due to its minimized size, high density, excellent electrical–mechanical performance and low power consumption [1, 2]. Through-silicon-via (TSV) and stacked chip interconnection which have involved with many times soldering processes is an important technology for 3D packaging [2]. During the fabrication of optical devices, micro electro-mechanical systems (MEMS) and bio-chips, the sensitive parts in those devices will be damaged if a high soldering temperature is used. Furthermore, the wafer warping issue due to the coefficient of thermal expansion (CTE) mismatch among different layers will be introduced at high bonding temperature. The low temperature bonding process is a promising way to solve above mentioned problems [3–10]. Unfortunately, the accompanying problem is that the solder bumps used in high density packaging generally have the diameters of 10 μm or less and thus the solder joints will be mainly composed by intermetallic compounds (IMCs) after subsequent multi-reflow processes, which will bring the thermal mismatch problem and consequently the solder joint failure [11]. The good news is that more IMCs also can bring the joint with better mechanical strength, high service temperature and other unexpected benefits, such as better electrical conductivity or thermal conductivity [12]. Hence, it is necessary to understand the story of IMC evolution in the small solder joint.

The existing chip interconnection technologies applied in 3D packages include: adhesive bonding, metal–metal thermocompression bonding, eutectic bonding, and wafer direct bonding. Niklaus et al. [13] have applied Benzocyclobutene (BCB) adhesive to wafer bonding but achieved relative low interconnection bonding strengths. Though thermocompression

bonding can get an Au–Au joint with the bonding strength of 30–50 Mpa [14], the gold material is too expensive and its processing compatibility with ICs manufacturing processes is unsatisfied. Cu–Cu thermo compression bonding method can bring the Cu–Cu joint with the joint strength of more than 50 Mpa [15, 16], but also requires high temperature and high pressure which are unacceptable in 3D packaging. Eutectic bonding method also requires high temperature and wafer direct bonding method requires very flat substrate surface which introduces great process complexity.

Inter chip via-solid liquid inter-diffusion (ICV–SLID) bonding method has been developed for 3D packaging, in which ICV provides vertical interconnections and SLID process offers the reliable mechanical–electrical interconnections under a low bonding temperature. The low melting point solder materials, such as Sn, SnIn, et al. have been used to interconnect Cu–Cu. Cao et al. [17] has investigated the effects of Sn layer thickness on solder joint reliability. They found that Sn could completely react with Cu to form IMCs when the reflow time was long enough. Yu et al. [18] has deposited the micron-scale In/Sn/Cu multilayers on a plate surface to fabricate $Cu_6(SnIn)_5$ IMC solder joints but found the reaction in the system was incomplete. Kato et al. [19] found that the thicknesses of Cu_6Sn_5 (η) and Cu_3Sn (ε) layers in Cu/Sn/Cu system were proportional to the square root of bonding time. When Sn layer was 5 μm, Sn was completely consumed after 20 min bonding. Only Cu_3Sn (ε) phase was remained at the interfaces after bonding for 300 min. Unfortunately, up to now the understanding of the IMCs evolution in a solder joint during solid–liquid interdiffusion low temperature bonding is still uncertain.

In this study, solid–liquid interdiffusion bonding method was applied to bond the Cu/Sn/Cu joint. For the convenience of sample preparation, the applied joints in this study were still with the scale of hundreds of microns. Within such big joints, the IMC fractions in the joints would be less if the normal reflow process was used. To be beneficial to simulate the real IMC evolution in small solder joints (a few microns), a long reflow time which was much longer than the normal reflow time was selected for the reflow process. With longer reflow time, the pure IMC joint can be obtained even within the joint with the size of hundreds of microns. The IMC morphologies, microstructure evolution, and grain orientation distributions during different reflow periods were investigated. Formation mechanism of pure IMC solder joints was also discussed to further understand the mechanism of solid–liquid interdiffusion low temperature bonding.

2 Experimental materials and method

The common material combination of high melting point metal (Cu) and low melting point solder material (Sn) were used in this study to fabricate the sandwich structure Cu/Sn/Cu joint. The Cu sheet with the size of $3 \times 3 \times 1$ mm^3 was used as the Cu substrate. A Sn foil with the thickness of 30 μm was used as the interlayer. The polishing process was applied on Cu sheets to obtain the clean and flat surfaces. After alignment, the sandwich structure was heated up to the temperatures which were higher than the melting point of Sn (232 °C). Then Cu atoms started to diffuse into the molten solder material and the solid–liquid interdiffusion process thus occurred. Sn gradually reacted with Cu to form Cu_6Sn_5 on the top of Cu substrate and then the Cu_6Sn_5 reacted with Cu to produce Cu_3Sn. After Cu_6Sn_5 was completely consumed, the solder joint would only be composed by Cu_3Sn.

With the process optimization, 0.05N was found to be the optimum bonding pressure to achieve the flat bonding interfaces. The sandwich structures were bonded under 240 and 300 °C with different reflow times of 25, 120, 240, 480, 720, and 960 min, respectively. Figure 1 shows the schematic illustration of the bonding process. To investigate the microstructures, the joints were prepared by standard metallographic analysis technology and the IMCs were observed using scanning electron microscopy (SEM). The IMC compositions were analyzed by energy-dispersive X-ray spectroscopy (EDXS). Electron backscatter diffraction (EBSD) technology was employed to reveal the grain boundaries and IMCs crystal orientations. To reveal 3-D morphologies of IMCs, the solder joints were split by melting method. Deep etching process was used to remove the residual Sn in the split joints.

3 Experimental results and discussion

3.1 Phase transformation of the Cu/Sn/Cu joints during bonding process

Figure 2 presents SEM images of Cu/Sn/Cu interfacial phase transformation with different bonding times under 240 °C. A thin layer of scallop Cu_6Sn_5 IMC was found at Cu–Sn interface after 25 min (Fig. 2a). At 120 min (Fig. 2b), Cu_3Sn occurred between Cu_6Sn_5 IMCs and Cu substrate. Obviously, the Cu_3Sn was the product of $1/20(Cu_6Sn_5 + 9Cu) = 1/4(Cu_3Sn)$ [20]. The thickness of Cu_3Sn phase increased with the time. The interface between Cu_6Sn_5 layer and Cu_3Sn phases was planar. With longer reflow time, the scallop Cu_6Sn_5 grains appeared nearby the residual Sn in the middle of the joint (Fig. 2c). By 480 min (Fig. 2d), the Cu_6Sn_5 IMCs from top and bottom Cu substrates contacted with each other and isolated the residual Sn into some separate areas (Fig. 2e). With the time more than 720 min, all Sn has been consumed and only Cu/Sn IMCs were left inside the joint, as

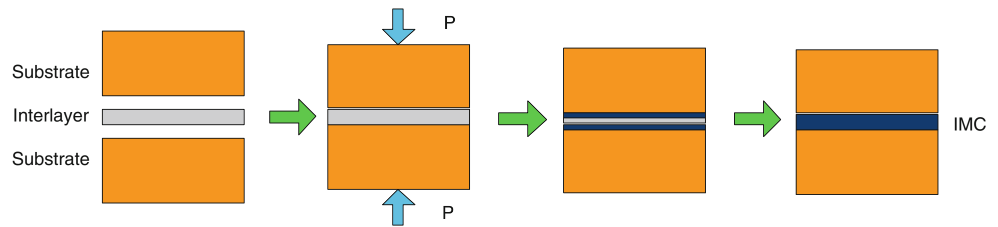

Fig. 1 Schematic drawing of the SLID process for Cu/Sn/Cu structure

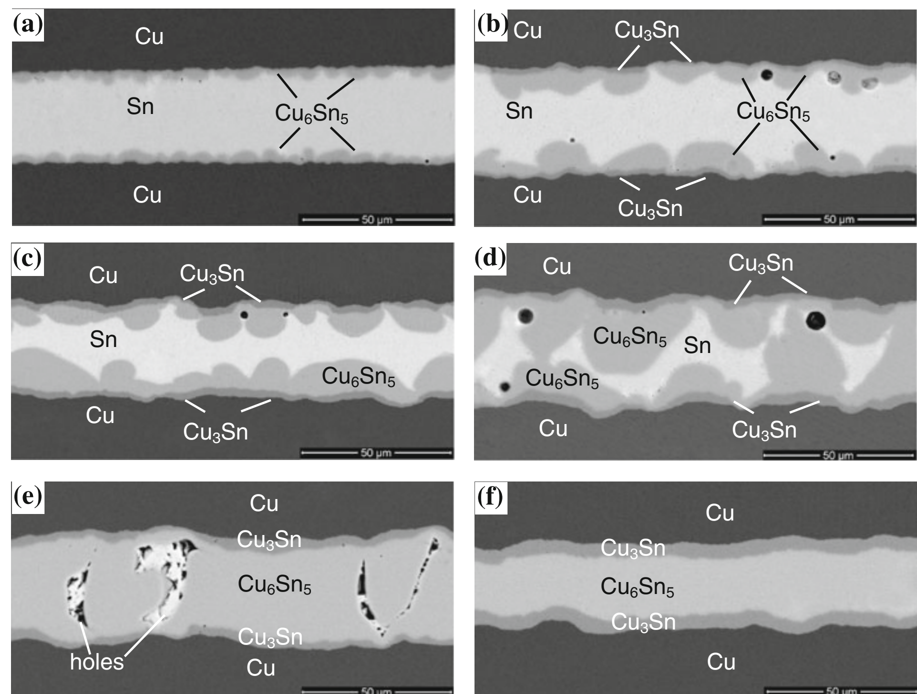

Fig. 2 SEM images of cross-sectional joints with different reflow times at 240 °C. **a** 25, **b** 120, **c** 240, **d** 480, **e** 720, **f** 960 (min)

shown in Fig. 2f. The defects in the joints, such as holes, could be attributed to the volume shrinkage during IMCs formation. As it was not the main topic in this study, the formation of these defects was not discussed.

Figure 3 shows Cu/Sn/Cu interfacial phase transformation under 300 °C for different reflow times. Higher reflow temperature brought higher IMC growth rate. Cu_3Sn layers were observed when the time was 25 min, as shown in Fig. 3a. By 120 min, the continuous Cu_3Sn layers were formed, as shown in Fig. 3b. At 240 min, the Cu_6Sn_5 grains from top and bottom Cu substrates contacted, as shown in Fig. 3c. By 480 min, all Sn has been consumed and the solder joint was composed by Cu_3Sn and Cu_6Sn_5, as shown in Fig. 3d. With longer time, Cu_3Sn layer became thicker while Cu_6Sn_5 layer became thinner, as shown in Fig. 3e. By 960 min, Cu_6Sn_5 disappeared and the solder joint was only composed by Cu_3Sn, as shown in Fig. 3f.

3.2 Morphologies evolution of Cu–Sn IMCs in Cu/Sn/Cu joints

Cu–Sn IMC morphologies were observed to further understand the IMC growth behavior. It was found that IMC morphologies in Cu/Sn/Cu sandwich structure were quite different from those in Cu/Sn joint. In Cu/Sn joint, the Cu_6Sn_5 grain morphology was similar to what formed in the solder joint of SnAgCu or SnPb solder bumps on Cu metal pad, which was usually described as roof shape or scallop shape, as shown in Fig. 4a. However, the IMC in Cu/Sn/Cu sandwich structures exhibited differently morphologies, as shown in Fig. 4b. In addition to the scallop or roof-shape Cu_6Sn_5 grains, it was found a lot of small grains on the surface of big Cu_6Sn_5 grains. Composition of the small grains with the size of 1–2 μm was determined to be Cu_6Sn_5 by EDXS technology, as shown in Fig. 4c. From the cross-sectional image in Fig. 4d, it was clear that the small Cu_6Sn_5 grains were on the top of the big Cu_6Sn_5 grain. Basically, with the processing of the reaction of Cu and Sn, the big Cu_6Sn_5 grains would keep growing. However, the already formed grains have contacted with each other to be a IMCs layer which could be the diffusion barrier for Cu atoms [21]. In the IMCs layer, the big Cu_6Sn_5 grains still had different grain orientations and their preferential growth directions might be blocked by the adjacent grains. At other growth directions, the required energy would be much higher. There had such a possibility

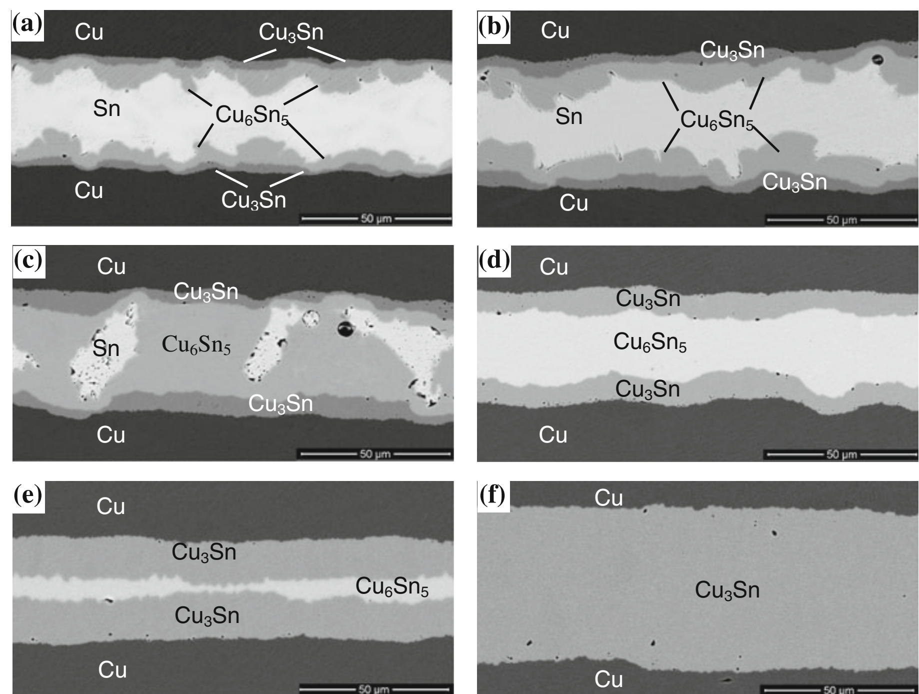

Fig. 3 SEM images of cross-sectional joints with different reflow times at 300 °C. **a** 25, **b** 120, **c** 240, **d** 480, **e** 720, **f** 960 (min)

that the nucleation energy of Cu_6Sn_5 grains was less than the required energy for the grain growth along those crystal directions (except the preferential growth direction) and hence new small Cu_6Sn_5 grains formed. The nucleation mechanism of small grains on big grain surface is uncertain for now and will be investigated in the future work.

Figure 5 shows the images of Cu_6Sn_5 morphologies in the joint after reflow process at 240 °C with 120 min. As the reaction process of Cu_6Sn_5 in different areas of the joint was not exactly the same, the Cu_6Sn_5 grain morphologies in different areas were different from each other, which in return reflected the evolution process of Cu_6Sn_5 grains. After the formation of the big scallop Cu_6Sn_5 grains, some small Cu_6Sn_5 grains uniformly formed on the surface of the big scallop Cu_6Sn_5 grains, as shown in Fig. 5a. With more Cu atoms, the small grains grew up to be bigger grains, as shown in Fig. 5b. The small grains continued to grow up and contacted with each other, as shown in Fig. 5c. With further reaction, the adjacent small grains merged into one big Cu_6Sn_5 grain and covered the previous formed Cu_6Sn_5 grain, as shown in Fig. 5d. Though there has no obvious evidence weather the new formed grain has merged with the previous formed grain or not, the plane crystal faces which were the characteristics of hexagonal Cu_6Sn_5 grain have occurred in the new formed grains, as shown in Fig. 5e. Finally, more plane crystal faces formed at the surfaces of Cu_6Sn_5 grain, as shown in Fig. 5f. This phenomenon also was found in another condition of 270 °C (not shown here).The nucleation and growth behaviors of the small grains were similar to those of Sn dendrite in SnAgCu solder [22, 23]. In that case, the growth behaviors of Sn dendrite were controlled by nuclear energy and supercooling and the crystal growth direction was along the temperature gradient. Here the nucleation and growth behaviors of the small Cu_6Sn_5 grains were supposed to be controlled by the Cu atomic concentrations in the growth front. Though some Cu atoms would pass through the Cu_6Sn_5 layer, most of Cu flux which had higher diffusion rate would diffuse into the liquid Sn phases through the Cu_6Sn_5 grains boundaries [21]. The Cu atomic concentrations at the areas nearby the big Cu_6Sn_5 grains boundaries would be much higher and hence the small size Cu_6Sn_5 grains formed there, as indicated in Fig. 5a. With more Cu atoms, the small size grains kept, growing up and connected with each other and finally covered the original big Cu_6Sn_5 grains, as indicated in Fig. 5c–f.

Figure 6 shows IMCs morphologies in the joint formed at 300 °C for 720 min and 960 min. Under high temperature with long reflow time (720 min), the previously formed Cu_6Sn_5 grains gradually converted into Cu_3Sn. A thin layer of Cu_6Sn_5 was observed between the Cu_3Sn layers, as shown in Fig. 6a. The interface between Cu_6Sn_5 and Cu_3Sn was shown in Fig. 6b. The grain size of Cu_6Sn_5 was much bigger than that of Cu_3Sn. The Cu_3Sn grains appeared as the columnar shape and the average diameter of the columnar grains was 1–2 μm. With longer time (960 min), most of IMCs in the joint was Cu_3Sn. The columnar shape grain clusters were shown in Fig. 7a.The formed Cu_3Sn grains were found to have different grain orientations, as indicated in Fig. 7b.

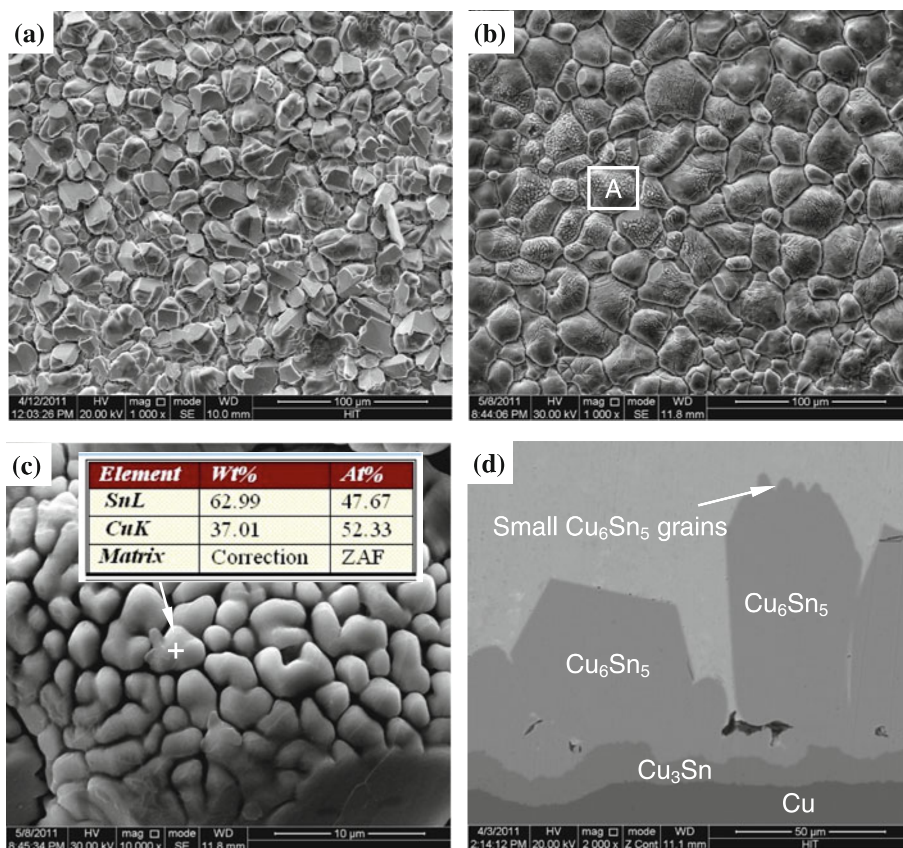

Fig. 4 Cu_6Sn_5 grain morphologies in singe-side joint and in sandwich joint at 240 °C for 480 min. **a** Cu/Sn joint, and **b** Cu/Sn/Cu joint, **c** Point A in b, **d** cross-sectional image of the Cu/Sn/Cu joint interface

3.3 Grain orientation of Cu–Sn IMCs in solder joints

EBSD technology was employed to investigate grain orientations and grain distributions in solder joints by point-to-point scanning mode. Figure 8a shows SEM image of the joint formed at 240 °C with 240 min. The areas with same color in EBSD grain mapping represented the same phase while the areas with different colors indicated different grains in the phase diagrams, as shown in Fig. 8b, c. It was found that the grains in the joint were Cu_3Sn, hexagonal Cu_6Sn_5, and tetragonal Sn, as indicated in Fig. 8c–e. With short reaction time and low temperature, a thin Cu_3Sn layer was observed nearby Cu substrate surface, as shown in Fig. 8b. In Fig. 8d, it was clear that the scallop Cu_6Sn_5 grains formed on same Cu substrate have contacted with each other. No preferred orientation relationship between Cu_6Sn_5 grains and the polycrystalline Cu substrate was found.

With longer time, the Cu_6Sn_5 grains from different Cu substrate surfaces continued to grow up and then contacted with each other at some areas, as indicated in Fig. 9a, b. The residual Sn occurred in the middle of the joint. Moreover, the thicknesses of Cu_3Sn layers at both sides became thicker. It was interesting that two Cu_6Sn_5 grains (at the top in Fig. 9d) were merged by different Cu_6Sn_5 grains from different Cu substrates. Before the Cu_6Sn_5 grains from different Cu substrates having been merged into one grain, the grains should have different grain orientations. However, the different orientations of different Cu_6Sn_5 grains have been changed to the same orientation during the merging stage. The merging process as well as the orientation change might also occur among the Cu_6Sn_5 grains formed on the same Cu substrate surface but with a significantly low merging rate.

The solder joint after Sn was totally consumed is presented in Fig. 10. The whole solder joint was composed by the Cu_6Sn_5 layer (middle) and the Cu_3Sn layers (side). With higher temperature and longer time, the pure IMCs joint formed. The thicknesses of Cu_3Sn layers at both sides were larger than that of the middle Cu_6Sn_5 layer, as shown in Fig. 10a, b). It was also found that there was only one Cu_6Sn_5 grain in the middle layer while there were lots of Cu_3Sn grains with different orientations in the side layers, as shown in Fig. 6c–e. The Cu_3Sn grains were columnar crystals with the grain sizes of 2–3 μm. Furthermore, the interfaces between Cu_6Sn_5 layer and Cu_3Sn layers still were planar. Before the formation of the continuous Cu_6Sn_5 layer in the middle of the joint, the merged Cu_6Sn_5 grains at different areas still had different grain orientations, as shown in Fig. 9d. After the different merged Cu_6Sn_5 grains started to remerge into bigger grains in the middle layer, the orientation change phenomenon occurred

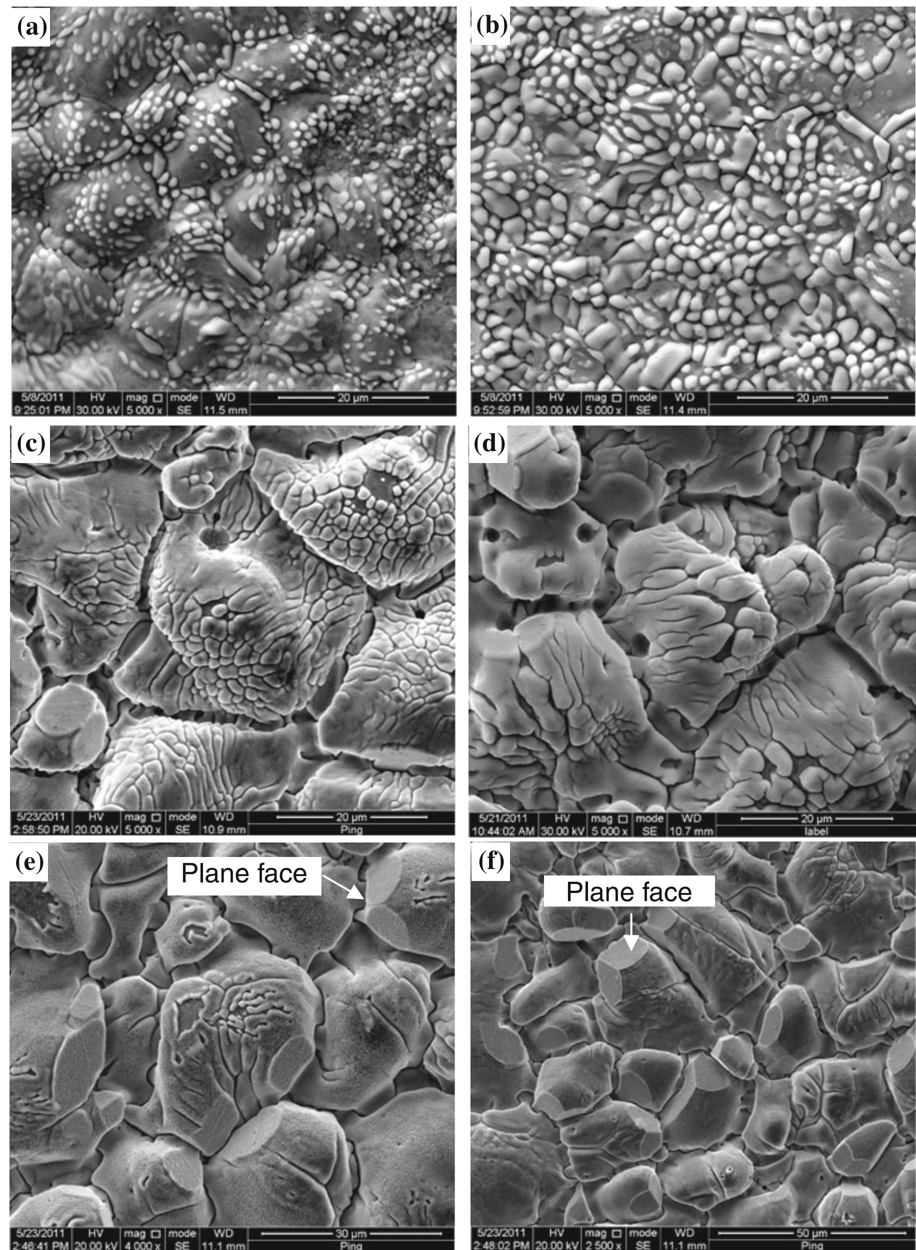

Fig. 5 Different Cu_6Sn_5 grain morphologies in the joint at 240 °C with 120 min

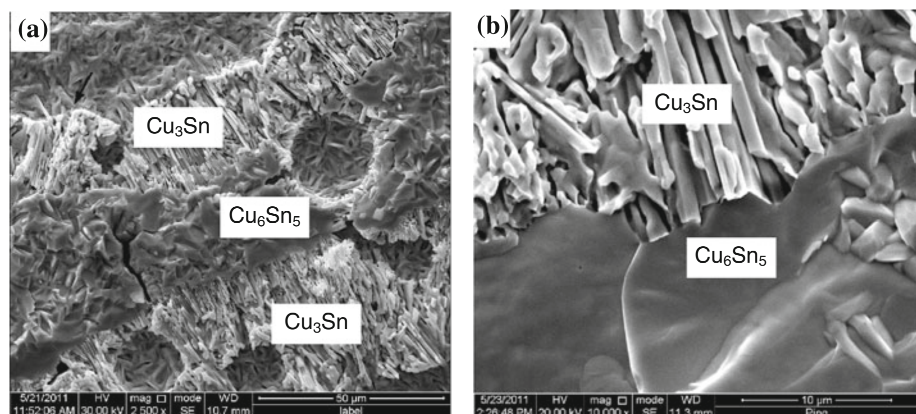

Fig. 6 Cross-sections of the joints at 300 °C for 720 min. **a** Cu_6Sn_5 and Cu_3Sn, **b** interface between Cu_6Sn_5 and Cu_3Sn

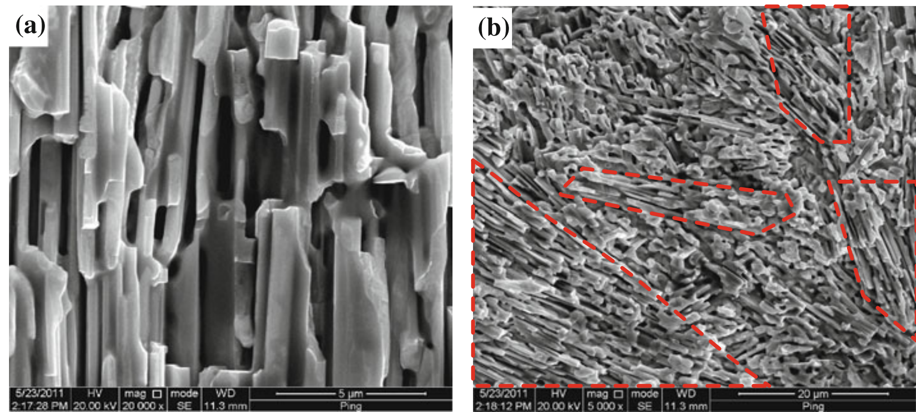

Fig. 7 Cross-sections of the joints at 300 °C for 960 min. **a** Cu_3Sn clusters, **b** different Cu_3Sn grains

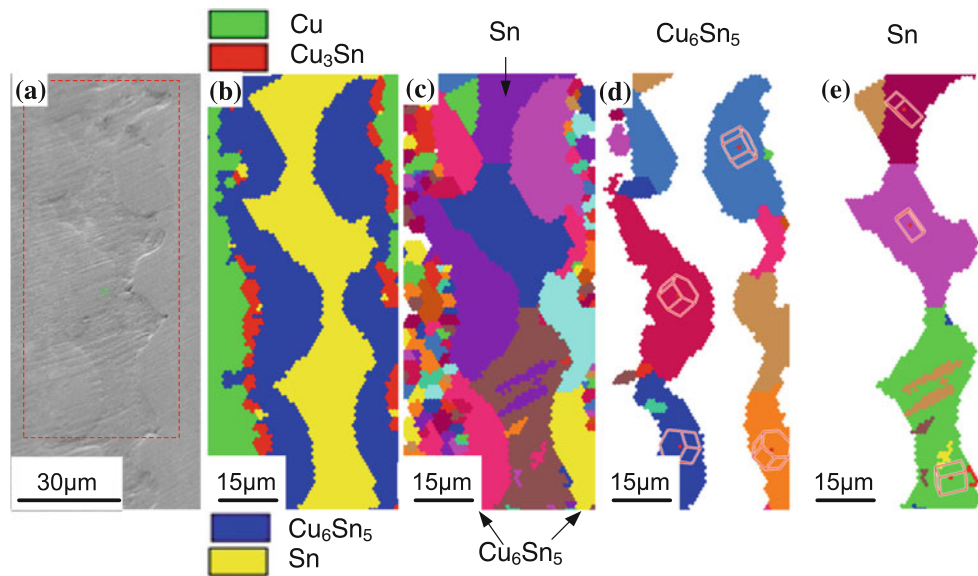

Fig. 8 Cross-sectional joint at 240 °C with 240 min. **a** SEM image, **b** EBSD mapping image, **c** Grain phase diagram, **d** Cu_6Sn_5, **e** Sn

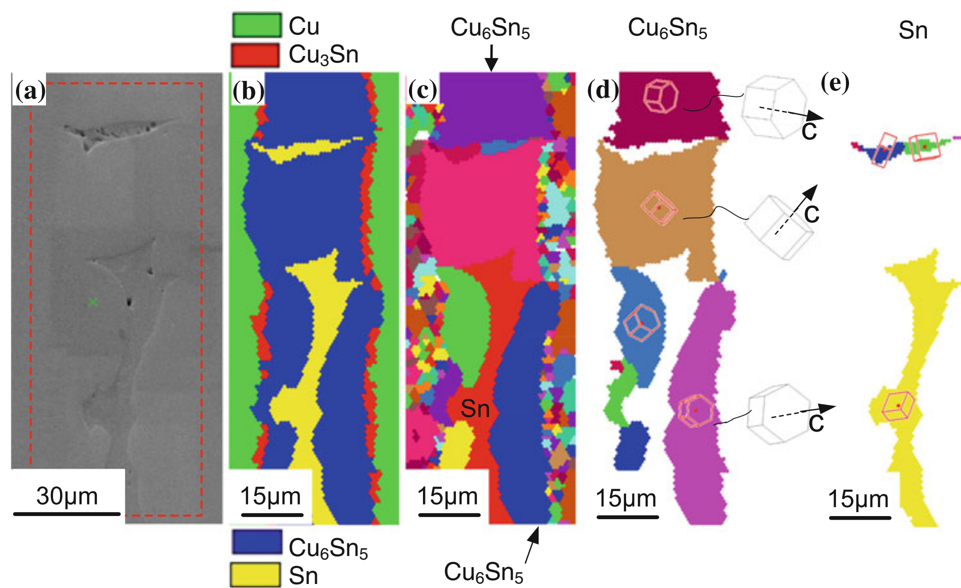

Fig. 9 Cross-sectional joint at 240 °C with 480 min. **a** SEM image, **b** EBSD mapping image, **c** Grain phase diagram, **d** Cu_6Sn_5, **e** Sn

again. The orientation change mechanism during grain merging process requires more investigations.

With 960 min at 300 °C, Cu_6Sn_5 was completely consumed and the only IMC phase in the joint was Cu_3Sn, as shown in Fig. 11a, b. There were a lot of Cu_3Sn grains in the joint, as indicated in Fig. 11c, which was different from that one single Cu_6Sn_5 grain in the middle layer in Fig. 10. Most of columnar Cu_3Sn grains were vertical to Cu substrate surfaces and the grain sizes were 2–5 μm. Absolutely, the influence from Cu grain orientations or Cu_6Sn_5 grain orientations on Cu_3Sn grain orientations was limited. As the Cu_3Sn grains grew up from different sides and failed to be merged into one big grain, a clear contact line was observed in the middle of the joint, as shown in Fig. 11c.

The growth behavior of IMCs in the sandwich structure joint was described in Fig. 12. Since the orientations of Cu grains in the polycrystalline Cu substrate are random, the

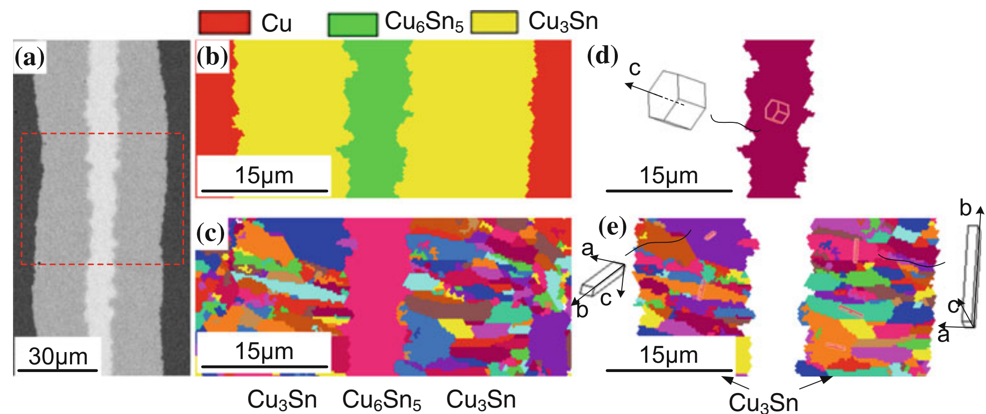

Fig. 10 Cross-sectional joint at 300 °C with 720 min. **a** SEM image, **b** EBSD mapping image, **c** Grain phase diagram, **d** Cu_6Sn_5, **e** Cu_3Sn

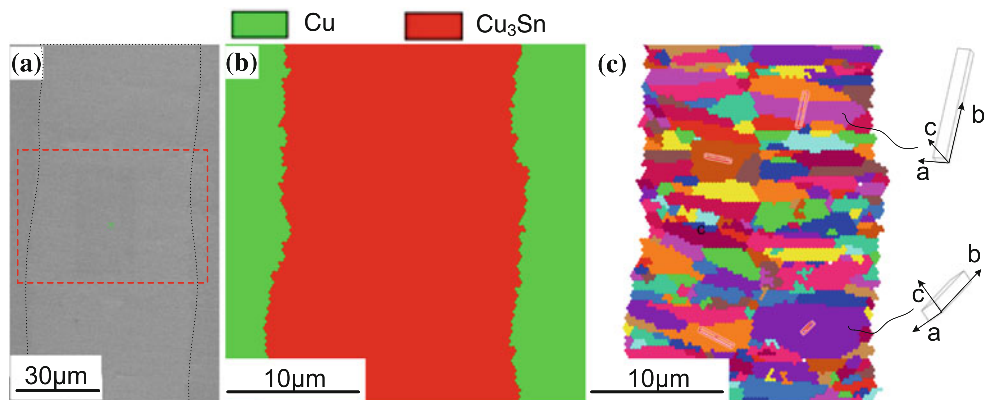

Fig. 11 Cross-sectional joint at 300 °C with 960 min. **a** SEM image, **b** EBSD mapping image, **c** Cu_3Sn

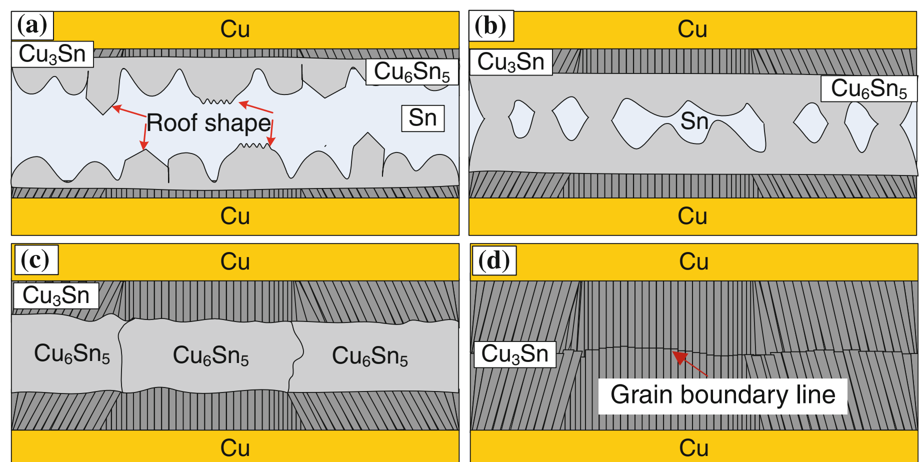

Fig. 12 Schematic drawing of IMCs evolution in Cu/Sn/Cu structure. **a** IMCs formation at the beginning stage, **b** Cu_6Sn_5 grains contacted, **c** IMCs without Sn, **d** Cu_3Sn

grain orientations of Cu_6Sn_5 formed on the Cu substrate surfaces are also random. The formed Cu_3Sn grains between Cu substrates and Cu_6Sn_5 layer also have different grains orientations. With longer reflow time, the Cu_6Sn_5 grains from different sides grow up and then are merged to be bigger grains. At the same time, the Cu_3Sn grains keep growing up with the original orientations. When Sn is completely consumed, the whole joint is composed by two Cu_3Sn layers and one Cu_6Sn_5 layer. The Cu_3Sn will keep growing up at the expense of the Cu_6Sn_5 depletion. With enough reflow time, the only IMC phase in the joint will be Cu_3Sn. The Cu_3Sn grains cannot be merged and the IMC grains still exhibit different grain orientations. Thus, the contact line will remain in the middle of the joint.

4 Conclusions

Phase transformation of the pure Cu–Sn IMC joint was obtained in Cu/Sn/Cu sandwich solder joint. Cu_6Sn_5 grains firstly formed and then gradually grew up to contact with each other. Cu_3Sn grains formed subsequently between the Cu_6Sn_5 layer and Cu substrates. The Cu_3Sn grains grew up at the expense of the depletion of Cu_6Sn_5. With longer time and higher temperature, the only IMC phase formed in the joint was Cu_3Sn.

The Cu_6Sn_5 grains with different grain orientations formed at the Cu substrate surfaces at the beginning stage. When the Cu_6Sn_5 grains from different substrates contacted, the grain merging as well as the orientation change phenomenon occurred and the different Cu_6Sn_5 grains with different grain orientations have been merged to be bigger grains. Despite the influences from the Cu grain orientations or Cu_6Sn_5 grain orientations, most of columnar Cu_3Sn grains were vertical to Cu substrate surface and the grain sizes were 1–5 μm. The grain merging phenomenon did not occur in Cu_3Sn grains. A contact line in the middle of the joint was observed when the Cu_6Sn_5 was completely consumed.

Acknowledgments This work has been supported by the National Science Foundation of China (Grant No. 51075103). Authors are grateful to the projects (HIT. NSRIF 2010120) supported by Natural Scientific Research Innovation Foundation in Harbin Institute of Technology.

References

1. C.T. Ko, K.N. Chen, Microelectron. Reliab. **50**, 481 (2010)
2. H. Huebner, S. Penka, B. Barchmann, M. Eigner, W. Gruber, M. Nobis, S. Janka, G. Kristen, M. Schneegans, Microelectron. Eng. **83**, 2155 (2006)
3. N.S. Bosco, F.W. Zok, Acta Mater. **52**, 2965 (2004)
4. J.S. Kim, P.J. Wang, C.C. Lee, IEEE Trans. Compon. Packag. Technol. **31**, 776 (2008)
5. C. Lee, A. Yu, L. Yan, H. Wang, J. He, Q. Zhang, J. Lau, Sens. Actuators A **154**, 85 (2009)
6. J.F. Li, P.A. Agyakwa, C.M. Johnson, Acta Mater. **58**, 3429 (2010)
7. J.F. Li, P.A. Agyakwa, C.M. Johnson, Acta Mater. **59**, 1198 (2011)
8. S. Sommadossi, A.F. Guillermet, Intermetallics **15**, 912 (2007)
9. T. Takahashi, S. Komatsu, T. Kono, Electrochem. Solid State **12**, H263 (2009)
10. A.A. Wronkowska, A. Wronkowski, K. Kuklinski, M. Senski, L. Skowronski, Appl. Surf. Sci. **256**, 4839 (2010)
11. D.Q. Yu, C. Lee, L.L. Yan, M.L. Thew, J.H. Lau, J. Alloy Compd. **485**, 444 (2009)
12. M. Li, Z. Li, Y. Xiao, C. Wang, Appl. Phys. Lett. **102**, 094104 (2013)
13. F. Niklaus, R.J. Kumar, J.J. McMahon, J. Yu, J.Q. Lu, T.S. Cale, R.J. Gutmann, J. Electrochem. Soc. **153**, G291 (2006)
14. M.M.V. Taklo, P. Storas, K. Schjolberg-Henriksen, H.K. Hasting, H. Jakobsen, J. Micromech. Microeng. **14**, 884 (2004)
15. K.N. Chen, C.S. Tan, A. Fan, R. Reif, Electrochem. Solid State **7**, G14 (2004)
16. C.S. Tan, Microelectron. Eng. **87**, 682 (2010)
17. Y.H. Cao, W.G. Ning, L. Luo, IEEE Trans. Electron. Packag. Manuf. **32**, 125 (2009)
18. D.Q. Yu, C. Lee, L.L. Yan, W.K. Choi, A. Yu, J.H. Lau, Appl. Phys. Lett. **94**, 034105 (2009)
19. H. Kato, S. Horikawa, K. Kageyama, Mater. Sci. Technol. **15**, 851 (1999)
20. K.F. Dreyer, W.K. Neils, R.R. Chromik, D. Grosman, E.J. Cotts, Appl. Phys. Lett. **67**, 2795 (1995)
21. H.K. Kim, K.N. Tu, Phys. Rev. B **53**, 16027 (1996)
22. J.C. Gong, C.Q. Liu, P.P. Conway, V.V. Silberschmidt, Scripta Mater. **61**, 682 (2009)
23. J.C. Gong, C.Q. Liu, P.P. Conway, V.V. Silberschmidt, Acta Mater. **56**, 4291 (2008)